MODIS Clear Water Epsilons

Algorithm Theoretical Basis Document

ATBD 21

Version 5

26 April, 1999

Kendall L. Carder, Christopher Cattrall , and F. Robert Chen

Marine Science Department
University of South Florida
140 Seventh Avenue South
St. Petersburg, FL 33701
kcarder@monty.marine.usf.edu

.

TABLE OF CONTENTS

Preface

This document describes the present state of development of the algorithm for retrieving the absorption of light by iron-rich dust aerosols. This derived value may then be used to flag and improve the atmospheric correction and determination of water-leaving radiance in remote sensing images of relatively clear waters ([*chl a*] < 0.5 mg/m^3). Saharan dust absorbs inversely with wavelength for wavelengths shorter than approximately 620 nm; the correction is achieved using the clear-water radiance from CZCS methods over visible wavelengths; MODIS atmospheric corrections rely on 750 and 865 nm, wavelengths not affected by absorption of iron-rich aerosols. Measurements of optical depths, angular sky radiance and irradiance are being performed at Ft. Jefferson, Dry Tortugas, a clear-water site free of anthropogenic influences. A CIMEL sun/sky photometer, one of the AERONET instruments (*Holben et al. 1996*) is also operated at this location, providing corroborative radiometric and optical depth data. These measurements demonstrate how $\varepsilon(531,667)$ and $\varepsilon(551,667)$ can provide a flag for blue-absorbing aerosols in remote sensing images. When combined with Saharan dust climatology or observations of the clear water before and during the dust event, estimates of light absorption are possible when combined with AERONET optical depth data. In this manner, a more accurate retrieval of $L_w(412)$ and $L_w(443)$ may be obtained in the presence of absorbing aerosols, of prime importance in estimating chlorophyll pigment concentration and primary productivity within the water column. Furthermore, iron is an important micronutrient for ocean primary production. Identifying its presence and estimating its concentration will be post-launch research objectives that make use of the clear-water epsilons. The code has been successfully integrated with other MODIS Ocean Team ode at the University of Miami Using MODIS processing criteria and tested using SeaWiFS data.

Version 5 replaces 4, released in August 1997.

1.0 Introduction

Recent suggestions that iron concentrations may limit phytoplankton growth in oligotrophic waters (*Martin and Fitzwater 1988*) have led to several iron-enrichment investigations. Surges in plant productivity, chlorophyll pigment concentration, and biomass were observed after a major iron enrichment of 64 km^2 in the equatorial Pacific (*Martin et al. 1994*), and in waters near Hawai'i during a major pulse of iron-rich dust from Asia (*Young et al. 1991*). The latter study showed that a mere 10% iron dissolution of the aerosol particles while sinking through the water column would explain the observed systematic increases of plant production with depth and time. These results suggest that iron-bearing aerosols may be an important source of iron to plants in the oligotrophic ocean regions.

Elemental iron is found in crustal aerosols in approximately crustal ratios (~ 5.6%); its crustal enrichment factor is consistently near unity (*Rahn 1976; Patterson et al. 1980; Chester 1990*) over the world oceans, although it has been observed at greater than 1.5 in the northern latitudes (*Rahn 1976*), and 2-3 during dust pulse events (*Young et al. 1991*). Aeolian input to the oceans is believed to be responsible for 30-96% of the dissolved iron input to the photic zone of the Sargasso Sea and 16-76% to the central North Pacific gyre (*Duce 1986*).

Satellite sensors have improved markedly in sensitivity and accuracy, necessitating inclusion of formerly neglected optical effects such as multiple scattering (*Gordon and Castaño 1987*), whitecap reflectance (*Gordon and Wang 1994*), and more detailed analyses of aerosols exhibiting spectral scattering (*Gordon and Wang 1994*). The complicated nature of these combined effects has led to common use of Monte Carlo radiative transfer schemes with standard aerosol models, generating look-up tables (LUT's) that afford quick and efficient atmospheric correction (*Gordon and Wang 1994; Reinersman and Carder 1995*). The most recent aerosol modeling work for satellite images (*Wang and Gordon 1993; Gordon and Wang 1994; Wang and Gordon 1995*) use the maritime, coastal, and tropospheric models provided by Shettle and Fenn (*Shettle and Fenn 1979*). All three models are formed using different ratios of two hygroscopic components: a relatively large (0.2 - 1.3 microns) oceanic particle with negligible absorption, and a smaller (r < 0.2 microns) urban particle that absorbs significantly ($0.959 \le \omega_a \le 0.989$), yet evenly, across the visible spectrum.

These radiative transfer calculations have accounted for absorbing aerosols by utilizing a non-spectral imaginary index of refraction. Desert dust such as that from the Saharan or Gobi deserts, however, often contain iron in oxide form which can cause distinct colour variations. In fact, iron is the element most responsible for the colour of dust (*Hurst 1977; Patterson 1981*). Saharan dust, for example, often absorbs far more strongly in the blue wavelengths than the yellow and red (*Lindberg and Laude 1974;*

Patterson 1981), resulting in a reddish-brown aerosol. Saharan dust is swept in vast quantities into the air streams over the west African coast in the dry summer months, and transported thousands of miles across the Atlantic Ocean to the Caribbean and eastern United States (*Schütz et al. 1981*). During the spring months, Gobi desert dust spreads across the Japan Sea and out over the North Pacific (*Darzi and Winchester 1982; Merrill et al. 1985; Betzer et al. 1988*). Such instances of high dust load in the atmosphere often confound satellite imagery by possessing optical signatures not completely accounted for using present atmospheric correction schemes, providing incorrect determinations of the water-leaving radiance (*Carder et al. 1991*). Accurate determination of the water-leaving radiance in the blue spectrum is of crucial importance in determining the chlorophyll pigment concentration and primary production within oceanic environments.

The primary purpose of this algorithm is to contrast a measured epsilon value, $\varepsilon(531,667)$, over clear waters to estimate aerosol iron content. In addition, for regions where $\varepsilon(531,667)$ is significantly less than $\varepsilon(750,865)$, the standard MODIS $L_{wn}(\lambda)$ values at shorter wavelengths will be suspect due to the blue-absorbing aerosols. Thus, a second purpose of this algorithm is to recalculate such suspect $L_{wn}(\lambda)$ values using the clear-water epsilon technique. Last, since these effects will not be discernible from Angström exponents derived using ratios of longer wavelengths, $\varepsilon(531,667)$ can also provide a check on the Angström exponent derived at red and infra-red wavelengths.

The method for obtaining clear-water epsilon values (Gordon and Clark, 1981; Gordon et al., 1983) have been thoroughly documented in the CZCS literature. No significant alterations to this earlier approach have been applied other than the extension of the clear water concept to include waters with higher pigment concentrations. We did modify the values of the normalized water-leaving radiance at 520, 550, and 670 nm for CZCS to the slightly different MODIS bands by means of the water absorption curve.

2.0 Overview and Background Information

One goal of MODIS is the determination of the chlorophyll pigment concentration within a 35% error. This ability rests squarely upon the accuracy of the water-leaving radiance retrievals. The strong absorption of blue light by dust aerosols will seriously undermine this effort if not detected.

2.1 Experimental Objectives

The objectives of this experiment are two-fold: 1) to provide a means of identifying blue-absorbing aerosols over clear waters and to estimate the iron flux to the ocean via these aerosols, and 2) to flag instances when L_{wn} retrievals may need adjustment due to aerosol absorption at blue and green wavelengths. Such errors will affect calculations of *[chl a]* using MODIS.

2.2 Historical Perspective

The success of the CZCS atmospheric correction algorithm in estimating and removing atmospheric effects is evident from its ability to determine the water-leaving radiance within about 10% for much of the world oceans, and chlorophyll concentrations to within approximately 40% under optimal conditions (*Gordon et al. 1983*). The flurry of research initiated by the success of the CZCS and improved remote sensing technology have led to vastly increased expectations and greater hopes for the next generation of ocean-viewing color sensors. MODIS will have a better radiometric sensitivity than CZCS due to a larger signal-to- noise ratio and a 12-bit digitization as compared with the 8-bit CZCS. This has necessitated the consideration of the full complexities of multiple scattering, oceanic whitecaps, earth curvature, and improved aerosol modeling (*Gordon and Wang 1992; Gordon and Wang 1994*).

2.3 Instrument Characteristics

The MODIS radiometric specifications are included in Table 1, after [Gordon, 1994 #256]. The noise equivalent reflectance ($NE\Delta\rho$) is derived using a solar angle of 60° and taken at the scan edge in order to simulate the least favourable viewing geometry. In addition to CZCS channels, MODIS has been equipped with a 412 nm band for separating the detrital and viable phytoplankton signals, and two bands centered on 750 and 865 nm to aid in atmospheric correction.

Band	Bandwidth [center]	$\rho_t(sr^{-1})$ ($\theta_o = 60°$)	NEΔL (sr^{-1})	NE$\Delta\rho$ (sr^{-1})	Required SNR
8	405-420 [412]	0.34	0.000052	0.00018	880
9	438-448 [443]	0.29	0.000050	0.00016	838
10	483-493 [490]	0.23	0.000043	0.00014	802
11	526-536 [531]	0.19	0.000041	0.00013	754
12	546-556 [551]	0.154	0.000030	0.00010	750
13	662-672 [667]	0.105	0.0000097	0.00004	910
14	673-683 [681]	0.105	0.0000094	0.00004	1087
15	743-753 [750]	0.081	0.000017	0.000085	586
16	862-877 [865]	0.069	0.000012	0.000076	516

Table 1

To recover the normalized water-leaving reflectance in the blue to within < 5% requires the accuracy of atmospheric correction to be within ±0.001 - 0.002 in reflectance at 443 nm (*Gordon 1996*).

3.0 Algorithm Development and Description

An introduction to both the historical and recent methods of atmospheric correction are required in order to appreciate the meaning of the spectral behaviour of absorption of dust aerosols. Thus, CZCS and MODIS correction schemes will be briefly touched upon before discussing aerosol absorption. Our notation duplicates that of the MOD-18 ATBD, where a complete description of the theory and nomenclature may be obtained. The single-scattering approximation will be used here until a Saharan dust model has been determined by our ground-based observations that may then be used as input to our radiative transfer code to effect the full multiple scattering solution.

3.1 Physics of the Problem

Up to 90% of the total radiance received at the sensor for most cloud-free scenes is due to the intervening atmosphere (Gordon et al., 1983). Aerosol scattering may be responsible for 10 to 40% of the radiance. Scattering by aerosols thus represents an important optical component of the atmosphere which must be removed from MODIS imagery before water-leaving radiances, hence chlorophyll, can be determined. Furthermore, aerosol concentrations and optical characteristics vary in both time and space. Thus the contribution of backscattered radiance by aerosols to the total radiance observed by the sensor cannot be estimated and removed *a priori*, as can the contribution by Rayleigh scattering.

Essentially, the single-component atmospheric correction algorithm rests on quasi-single scattering theory and the clear water radiance technique (Gordon and Clark, 1981; Gordon et al., 1983). Single scattering theory allows Rayleigh scattering radiance (L_r), aerosol scattering radiance (L_a), and water-leaving radiance (L_w) to be separated. The clear-water radiance technique utilizes *a priori* knowledge of the water-leaving radiance of low-chlorophyll sea water at 531, 551, and 667 nm to calculate the contribution of aerosol scattering to the total radiance received at the sensor (L_t) at each of the wavelengths. The water-leaving radiance at 443 nm (the band most sensitive to chlorophyll absorption) is then determined through extrapolation of the aerosol radiance to 443 nm. Treatment of the Rayleigh and aerosol scattering in a single scattering sense (i.e., as independent terms) results in errors in aerosol radiance values less than 10% for aerosol optical thicknesses (τ_a) less than 0.6 under most conditions with non-absorbing aerosols (Gordon et al., 1983).

3.2 Atmospheric Correction

Radiance resulting from scattering is denoted in the literature by $L_x(\lambda)$, *x* representing the source of the scattered signal, such as Rayleigh (*r),* aerosol (*a*), or multiple (*ar*, *ra*) scattering. It is more convenient and physically meaningful to use *reflectance* (*Gordon and Clark 1981*) (θ_o representing the solar zenith angle and F_0 the extraterrestrial solar irradiance),

$$\rho_x(\lambda) = \frac{\pi}{F_o(\lambda) \cdot \cos\theta_o} L_x(\lambda)$$

The complete formulation of the correction algorithms have been thoroughly documented (*Gordon and Clark 1981; Gordon et al. 1988; Gordon and Wang 1994*) and shall not be reviewed here. The quantity of importance is the ratio of aerosol reflectances (denoted by *as*) received by the sensor at wavelengths λ_i and λ_j and a viewing angle θ_v:

$$\varepsilon(\lambda_i, \lambda_j) \equiv \frac{\rho_{as}(\lambda_i)}{\rho_{as}(\lambda_j)} = \frac{\omega_a(\lambda_i) \cdot \tau_a(\lambda_i) \cdot p_a(\theta_v, \phi_v; \theta_o, \phi_o; \lambda_i)}{\omega_a(\lambda_j) \cdot \tau_a(\lambda_j) \cdot p_a(\theta_v, \phi_v; \theta_o, \phi_o; \lambda_j)}$$

The parameters $\tau_a(\lambda)$, $\omega_a(\lambda)$, and p_a are, respectively, the aerosol optical thickness, single-scattering albedo, and aerosol scattering phase function. Physically, $\varepsilon(\lambda_i, \lambda_j)$ represents the relative strengths of the aerosol scattering and absorption, largely independent of the power of the light incident upon the aerosol particles, viewing geometry, and the concentration of aerosol particles present.

For large, iron-rich, desert dust particles, the ratio of aerosol reflectances at 550 nm and 670 nm, $\varepsilon(550, 670)$, has been shown using CZCS data to decrease to 0.94 and below (*Carder et al. 1991*) during strong dust events; typical values of 1.0-1.5 are found for smaller, non-iron-bearing aerosols. In such occurrences, when aerosol reflectance is lower in the blue than the green or red, strong absorption is likely present.

Assuming complete avoidance of sun glitter, the total reflectance received at an ocean-viewing sensor can be described by:

$$\rho_t(\lambda) = \rho_r(\lambda) + \rho_a(\lambda) + \rho_{ra}(\lambda) + t(\lambda) \cdot \left[\rho_{wc}(\lambda) + \rho_w(\lambda)\right], \text{ where}$$

$$t(\lambda) = e^{-(\tau_R(\lambda)/2 + \tau_{OZ}(\lambda) + (1 - \omega_{as}(\lambda) \cdot F)\tau_{as}(\lambda))/\cos\theta_o}$$

The subscripts represent the contributions from Rayleigh scattering, aerosol interactions (absorption *and* scattering), Rayleigh-aerosol interactions, whitecaps, and water-leaving radiance, respectively, and *F* the probability of forward scattering. Rayleigh scattering and whitecap reflectance may be determined *a priori* with knowledge of sun and spacecraft zenith angles and wind velocity. The diffuse transmittance of the atmosphere, $t(\lambda)$, is considered known since it is primarily a function of Rayleigh and ozone optical thickness (τ_r and τ_{oz}) and the satellite zenith viewing angle, θ_v, and only secondarily a function of aerosol attenuation (*Gordon et al. 1983*). Thus, separation of the total signal into components is reduced to that of determining the aerosol and water-leaving radiances.

3.2.1 CZCS

Separation of $\rho_w(\lambda)$ and $\rho_{as}(\lambda)$ was effected for the CZCS using quasi-single scattering theory and clear-water radiances (*Gordon and Clark 1981*). The basis for this theory is that where chlorophyll *a* plus pheophytin *a* concentrations (C) are less than 0.25 mg m^{-3}, the normalized water-leaving radiances, $L_{wn}(\lambda_i)$ can be designated *a priori* to within 10%. At 520, 550, and 670 nm these values are 0.495, 0.28, and less than 0.015 mW cm^{-2} μm^{-1} sr^{-1}, respectively. Thus, $\varepsilon(520,670)$ and $\varepsilon(550,670)$ were determined over clear water. For a given wavelength, $L_w(\lambda_i)$ can be related to $L_{wn}(\lambda_i)$ through

$$L_w(\lambda_i) = L_{wn}(\lambda_i)t(\theta_o,\lambda_i)\cos\theta_o$$

Clear-water radiances now determine $\rho_\omega(520)$, $\rho_\omega(550)$ and $\rho_\omega(670)$, yielding $\rho_{as}(\lambda)$ for these wavelengths at each pixel in a clear-water region (presumed to include most ocean regions away from land and within 35° latitude from the equator). Using the assumption that the aerosol size distribution behaved according to (*Junge 1963*),

$$\frac{dn(a)}{da} = C(z)\cdot a^{\gamma},$$

where *n* is the aerosol particle number density, *a* the particle radius and γ the Junge parameter, the aerosol optical depth is given by (*Van de Hulst 1957; Gregg and Carder 1990*):

$$\tau_a(\lambda) = K\cdot\lambda^{-(\gamma+3)}$$

$$= K\cdot\lambda^{-\eta_\tau(\lambda)},\ \eta_\tau = \gamma + 3 \text{ (Angström exponent)}$$

A further assumption of a single scattering albedo of unity and non-spectral phase functions gives the aerosol epsilon:

$$\varepsilon(\lambda_i,\lambda_j)=\frac{\rho_{as}(\lambda_i)}{\rho_{as}(\lambda_j)}=\left(\frac{\lambda_i}{\lambda_j}\right)^{-\eta_\tau(\lambda_i)}$$

The epsilon values $\varepsilon(\lambda_i,670)$ derived for spectral bands 2, 3, and 4 are spatially averaged and used to "type" the aerosol by determining an average Angström exponent, allowing $\varepsilon(443,670)$ to be determined. This method is usually applied to a 5-by-5 pixel region of a clear water portion of the scene to increase the signal-to-noise ratio. $\rho_w(443)$ is then determined by,

$$\rho_w(443)=\frac{1}{t(\lambda)}\left[\rho_t(443)-\rho_r(443)-\varepsilon(443,670)\cdot\rho_{as}(670)\right]$$

Treatment of the Rayleigh and aerosol scattering in a single-scattering manner results in errors in aerosol radiance values less than 10% for aerosol optical thickness (τ_a) less than 0.6, under most conditions (*Gordon et al. 1983*).

3.2.2 MODIS

While the Angström formulation was sufficiently accurate from 520-670 nm, the CZCS wavelength range, Monte Carlo simulations using published values of aerosol size distributions and refractive indices (*Shettle and Fenn 1979*) at varying wavelengths, scan geometries, and relative humidities have shown that over the MODIS range 531-865 nm this formulation was a poor approximation (*Gordon 1996*). Gordon's results suggest

$$\varepsilon(\lambda_i,\lambda_j)=e^{c(\lambda_j-\lambda_i)},$$

where *c* is a constant depending on aerosol model and relative humidity, would be a more accurate parametrization of the problem.

Aerosol reflectances may be obtained over clear water at 750 and 865 nm since the water-leaving radiances are zero, providing a determination of the constant *c*. This parametrizes the aerosol reflectances over all wavelengths. Note this stems purely from the signals received at 750 and 865 nm, an area of the spectrum normally exhibiting negligible absorption by iron-rich mineral aerosols. An aerosol with optical

signatures exhibiting differing spectral dependence will confound this method further than the CZCS approach, which uses visible channels in the atmospheric correction.

3.2.3 Aerosol Absorption

The phase function to be used in radiative transfer modeling is often simulated using Mie scattering theory, based upon spherical particles. The optical depth can be expressed with knowledge of the complex index of refraction of the aerosol particles, $m = n_{RE}(\lambda) - in_{IM}(\lambda)$ (*Van de Hulst 1957; D'Almeida et al. 1991*) by:

$$\tau_{as}(\lambda) = \int_{z_1}^{z_2} \left\{ a(z,\lambda) + b(z,\lambda) \right\} \cdot dz, \qquad \text{where} \quad a(\lambda), b(\lambda) = \int_{r_1}^{r_2} Q_{a,b}(m,r,\lambda) \cdot \pi r^2 \cdot \frac{dN(r)}{d\ln(r)} \cdot dr$$

$Q_{a,b}$ are the dimensionless absorption and scattering efficiencies determined by Mie theory. Thus, the relative strengths of absorption and scattering by the atmospheric aerosol will depend upon the particle size distribution, index of refraction, and concentration.

Our initial investigations set aside direct measurements of particle concentration and size distributions and focus on observing the *in-situ* bulk absorption coefficient,

$$a(\lambda) = \frac{4\pi \cdot n_{IM}(\lambda)}{\lambda}$$

The optical properties of crustal aerosols have been extensively studied at source and island sites distant from the origin of aerosol dust types (*Patterson and Gillette 1977; Patterson 1981*) using diffuse reflectance techniques. The imaginary index of refraction, n_{IM}, increases significantly in the blue compared to the red and green wavelengths. The n_{IM} of Saharan dust, for example, was observed to increase log-linearly over the wavelengths 600 to 400 nm., approximately following

$$n_{IM}(400{:}600) \propto 10^{m\lambda}, \text{ m} \sim -3.6 \text{ such that}$$

$$a(\lambda) = \frac{4\pi \cdot 10^{-3.6\lambda}}{\lambda} \propto 10^{-(3.6\lambda + \log\lambda)}.$$

Rural dust samples from Texas, Denver and an Asian desert also exhibit monotonically decreasing absorption with increasing wavelength over these ranges.

Thus, for dust whose absorptive tendencies can be predicted over a certain wavelength range, if the absorption may be determined at several wavelengths, a ready approximation for absorption at all wavelengths within that regime may be made.

3.3 Mathematical Description of the Algorithm

The increased sensitivity and accuracy of MODIS has necessitated inclusion of multiple scattering effects. The present approach (*Gordon 1996*) parametrizes the multiple scattering contribution to be proportional to the single-scattering aerosol reflectance:

$$\left[\rho_a(\lambda) + \rho_{ra}(\lambda)\right] = K[\lambda, \rho_{as}(\lambda)] \cdot \rho_{as}(\lambda)$$

The value of the proportionality constant $K[\lambda,\rho_{as}(\lambda)]$ is determined from a look-up table once the appropriate aerosol models, or combination of two aerosol models, and viewing geometry, have been determined. This method provides very good retrievals as long as the candidate aerosols are similar those actually present in the images. The presence of strong absorption, however, can greatly overestimate the atmospheric effect if the aerosol epsilon is calculated using inappropriate models (*Gordon 1996*). Gordon (1996) concludes that since a relationship between single scattering albedo, $\omega_a(\lambda)$, and $\varepsilon(\lambda_i,\lambda_l)$ cannot be determined from $\varepsilon(750, 865)$ it must be determined for each candidate aerosol model and applied based upon climatology.

The iron content and size distribution of Saharan dust, thus single-scattering albedo and phase function, vary widely both seasonally with the source region and synoptically with the local meteorology (*Arimoto et al. 1995*). Since a characteristic epsilon parametrization may not then exist, we developed a sensitive hyperspectral method for determining blue-light absorption from ground-based sky radiance and optical depth measurements taken during Saharan dust events. These radiometric measurements determine the phase function and spectral single-scattering albedo of long-range Saharan dust [$\omega_a(\lambda)$, $P(\Theta,\lambda)$] (see Appendix C for further details) *for each particular dust event.* We are performing scanning electron microscopy investigations of aerosol samples provided by D. Savoie at the University of Miami to determine the morphology, size distribution, and chemical composition of the aerosols present in each dust event for which optical parameters [$\omega_a(\lambda)$, $P(\Theta,\lambda)$, $\tau_a(\lambda)$] have been measured. We expect that a suite of epsilons, representing different instances of Saharan dust, will be obtained through,

$$\varepsilon(\lambda_i,865) \equiv \frac{\rho_{as}(\lambda_i)}{\rho_{as}(865)} = \frac{\omega_a(\lambda_i)\cdot\tau_a(\lambda_i)\cdot P(\Theta,\lambda_i)}{\omega_a(865)\cdot\tau_a(865)\cdot P(\Theta,865)},$$

where λ_i = 412, 443, 488, 531, 551, and 611 nm. These derived models may then be used as input to Monte Carlo radiative transfer code in order to construct the look-up table for K [λ,$\rho_{as}(\lambda)$], and to estimate the effect of light absorption by desert dust upon retrieved water-leaving radiances over oligotrophic waters.

The upper limit of ε(531, 667) has been set at 0.95 to flag blue-light absorbing aerosols, but will be refined once the field data has been analyzed, and the spectral behaviour of the aerosol epsilons has been characterized. Oligotrophic waters are not expected to evince rapid changes in chlorophyll pigment concentrations; water-leaving radiances may be observed in imagery before and during the dust event to note uncharacteristic changes or values.

3.4 Practical Considerations

Knowledge of ε(531,667), ε(551, 667) will likely be enough to flag absorbing aerosols. Estimation of absorption may also be possible purely from the radiometric satellite data using a Look-Up Table (LUT). A good knowledge, however, of the spectral variation of aerosol optical depths would provide a firmer basis for estimating aerosol size distribution. This information may be obtained from the CIMEL sun/sky photometer network, AERONET (*Holben et al. 1996*). The CIMEL network is attractive because many stations already exist in continuous operation, and the data is readily available from Goddard. Thus, SeaWiFS and CIMEL data may be used as a test-bed for this MODIS algorithm.

An unknown aerosol vertical structure causes significant error in the atmospheric correction when strongly absorbing aerosols are present (*Gordon 1996*). Vertical distribution climatology is desirable and possible with the Lidar In-space Technology Experiment (LITE) (*Winker et al. 1996*). Observations of Saharan dust transport have already been made, with the observed Saharan Air Layer (SAL) residing 1-5 km in height near the West African coast, and near 3 km altitude in the western Atlantic at which height it is less distinguishible from the marine boundary layer (*Powell et al. 1996*).

3.4.1 Numerical computational considerations

We modified the normalized water-leaving radiances, $L_{wn}(\lambda_i)$, at 520, 550, and 670 nm (which are designated *a priori* for the CZCS) to 531, 551, and 667 nm for MODIS by

$$L_{wn}(531) = \frac{a_w(520)}{a_w(531)} L_{wn}(520)$$

$$L_{wn}(551) = L_{wn}(550)$$

$$L_{wn}(667) = \frac{a_w(670)}{a_w(667)} L_{wn}(670)$$

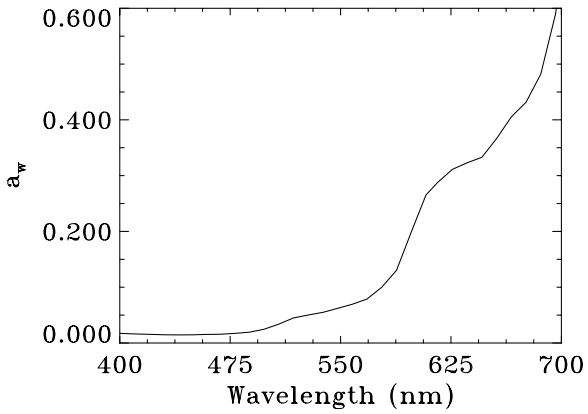

where $a_w(\lambda)$ are water absorption coefficients from Smith and Baker (1981).

3.4.2 Calibration and Validation

Aerosol Angström exponents and epsilons are estimated from skylight backscattering measurements at large solar zenith angles taken on clear days, and days where the aerosol signal is dominated by dust using a 512 channel spectroradiometer. Aerosol optical thicknesses are determined using a 10-channel Reagan radiometer. Spectral irradiance is collected by scanning a Spectralon greycard of known reflectance with the spectroradiometer, and corroborated with a LI-1800 irradiance meter. Side/back-scattering measurements of the atmosphere from the Florida Keys in winter will allow clear-water epsilons to be determined over the low chlorophyll waters of the Florida Current during which, or shortly after, ground-based sky radiance measurements are made. Occasional ship data of $L_w(\lambda)$ will be acquired to test the clear-water radiance assumptions. Appendix C provides a description of initial results of the data collection at Ft. Jefferson in the Dry Tortugas (Florida Keys).

3.4.3 Variance or uncertainty estimates

Uncertainties of less than 0.05 for ε(531,667) within the range 0.8 to 1.3 are estimated at present for clear-water regions.

A comparison of ε(531,667) with ε(750,865) is necessary to ascertain the sensitivity of epsilon at lower wavelengths to the presence of dust, compared to that of 750 nm. Its sensitivity to aerosol optical depths also needs to be quantified.

Error analysis and estimates will be misleading at this point; the indistinguishability of multiple interactions and pure absorption, and a possible incomplete removal of Rayleigh scattering would

obfuscate this issue. The clear absorption signature seen in the radiometric plots in Appendix C is strong evidence of an effective method, and has provided impetus for the next series of computations and fieldwork.

3.4.4 Quality Control and Diagnostics

We are currently collecting monthly data at Ft. Jefferson, a clear-water, clear-atmosphere island site in the Florida Keys. Other angular scattering measurements, irradiance measurements, and optical depth data will be dependent upon the distance from the terrestrial source from which the turbidity is generated. Size distribution and concentrations change dramatically as the dust moves away from the source; varying soil types have distinctly different chemical structure and composition, and size distributions. These differences will need to be carefully examined before incorporating outside date sets into our database, even after appropriate corrections for altitude, solar and viewing angles etc. An all-inclusive characterization of dust scattering data would in fact be undesirable and misleading; enough field research has been performed to distinguish optical properties of Gobi and Saharan desert dust, and other arid and/or rural soil samples.

3.4.5 Output product

The output product in its simplest form will be maps of the estimated light absorption, inferred iron content of aerosols over clear waters, and a flag for potential problems with L_w values calculated using Angström exponent-based extrapolations from the infra-red for aerosol radiance values in the visible. While 4 km spatially binned $\varepsilon(531,667)$ data would be sufficient for most science interests regarding iron flux, diagnosing potential problems with the L_w field may require full-resolution data.

We are extending the use of the "clear water" radiance approach to regions with chlorophyll concentrations as high as 0.5-1 mg m^{-3} (see Appendix A). This will dramatically increase the useful range of applicability of the algorithm with only a modest increase in the expected error (8% to 13%) in $L_{wn}(531)$. For major dust outbreaks where the major flux of iron to the ocean might be expected, $L_a(531)$ will be far greater than the increase in uncertainty in $L_{wn}(531)$.

3.4.6 Code Tests at the MODIS Ocean Team Computing Facility

An end-to-end test of the MODIS Ocean Team's software for deriving Level 2 to Level 4 products was conducted at the University of Miami by Dr. Robert Evans during winter-spring 1999.

The test used two days of SeaWiFS ocean color data and AVHRR sea-surface temperature data for the entire globe to evaluate the data volume, data flow, and to discover algorithm coding and performance errors.

The test was successful, providing variables required for calculating MOD22 products, IPAR and ARP on a global basis. We are actively testing the data set for the performance of data-quality flags to evaluate whether they are detecting all aberrations in input data quality and algorithm performance. Noting that MODIS will have even better signal-to-noise ratios and less absorbing gas effects on aerosol radiance retrievals, the success of this test is extremely encouraging.

3.4.7 Tests with SeaWiFS Data

Radiances from the top of the atmosphere were acquired for SeaWiFS scenes over the Sargasso Sea where the water-leaving radiances are well understood. For dust-rich scenes in June 1998 the $\varepsilon(\lambda,865)$ values behaved in a manner consistent with the backscattered sky radiance measured from the ground at the Fort Jefferson (see Appendix). The dust-rich reflectances were smaller at the blue end of the spectrum for large viewing angles than for a nearby, low-aerosol pixel. The effect suggests that not only is the single-scattering albedo well less than 0.9, but the aerosol absorbs significant fractions of the blue upwelling radiance from the ocean and air molecules as a multiple-scattering/interaction effect. This resulted at the blue ends of the spectrum in an effective $\varepsilon(\lambda, 865)$ for the aerosol radiance that appeared to decrease with decreasing λ as λ^{-5}. If the single-scattering albedo falls off with decreasing wavelength as λ^{-1}, then to obtain λ^{-5}, significant Rayleigh radiance must be absorbed. This is in complete agreement with the Figures shown in the Appendix for ground-based observations.

4.0 Constraints, Limitations and Assumptions

Gordon and Castaño (1987) have shown that errors associated with the quasi-single scattering model result from multiple scattering effects on $L_a(\lambda)$ and the assumed independence of $L_r(\lambda)$ and $L_a(\lambda)$. Therefore, when both the solar zenith angle and the Angström exponent are increased, care must be taken in interpreting the data, or else a multiple scattering model should be used.

When pigment concentrations are larger than 1 mg m^{-3} (to be extended to 2, see Appendix A), L_{wn} is no longer known for 531 and 551 nm so this method cannot be applied. Thus, the algorithm will be effective only over clear (open ocean) water

This algorithm will only be effective for dust that absorbs in a known and predictable manner over the wavelength range involved. Thus, an extensive database of optical signatures is being pursued.

Dust from the same source may have very different scattering and absorptive signatures during its transport phase; absorption by dust is due primarily to the smaller size fraction of aerosols, the clay mode, not quartz particles (*Savoie and Prospero 1976; Savoie 1978*). As the dust is transported away from the source, the quartz particles drop out of the air mass at a rate far greater than that of the light clay particles. The scattering and absorptive characteristics of a dust pulse will change markedly, for example, as it moves from the African Sahel to the southern tip of Florida (*Prospero 1981*). Such transport and settling mechanisms must be carefully considered in atmospheric correction of satellite imagery over oligotrophic waters.

The physics of the problem will be slightly different for a nadir-viewing sensor. The Rayleigh scattering term will be proportionately much larger as it is not attenuated by the aerosol layer. Dust absorption effects will comparatively be perhaps only 10-20% of that observed in ground-based measurements. Concomitantly, aerosol dust storms often extend to 6 km (*Betzer et al. 1988*), confounding the simplifying assumption of clearly-defined atmospheric layers. Monte Carlo simulations (*Reinersman and Carder 1995*) will be pursued in the near-future to examine such possible effects.

5.0 Research Timetable

Measurements will continue for two years at Ft. Jefferson in order to build a large database of optical signatures. Dust storms moving across the Atlantic are common in the late summer months, thus, collection will be concentrated during these times.

A Mie scattering code will be employed to simulate the phase function and albedo of different aerosol types and size distributions to effect a numerical closure of aerosol reflectances, single-scattering albedo, phase function, and optical depth.

An extensive MODIS aerosol measurement network is being developed using CIMEL solar and sky radiometers (ATBD MOD-04). Island measurements from CIMEL activities will also be useful for epsilon evaluation; such an instrument is currently operating at Ft. Jefferson and will provide corroboration of the measurements taken.

In order to investigate a large range of solar zenith angles, aerosol types and optical depths, other clear-water island areas will be included once the algorithm has performed satisfactorily. This will also aid in investigating the change in optical signature from the same dust source, such as the Gobi or Saharan Desert.

Data linking optical depths and radiance/irradiance measurements to aerosol chemical composition and concentrations are quite scarce. The University of South Florida has the ability to determine the concentration of trace elements present in the aerosol particles, and an X-ray diffraction capability that will aid in determining aerosol structure. Aerosol samples will be obtained from island sites such as the Canaries, Azores and Japan using aerosol collection towers already in place as our radiometric measurements are being taken. Lidar returns from Tokyo and Chiba universities can be taken simultaneously with our measurements. Aerosol samples also collected at the same time will lead to a comprehensive suite of measurements. Extensive efforts will be made to link top-of-the-atmosphere data (SeaWiFS and MODIS) with ground based measurements to improve our ability to detect and correct to first order scenes with desert dust, at least over clear waters.

References

Arimoto, R. R. A. Duce et al., Trace elements in the atmosphere over the North Atlantic, *Journ. Geophys. Res.* **100**(D1): 1199-1213, 1995.

Betzer, P. R. K. L. Carder et al., Long-range transport of giant mineral aerosol particles, *Nature* **336**(6199): 568-571, 1988.

Biggar, S. F. D. I. Gellman and P. N. Slater, Improved Evaluation of Optical Depth Components from Langley Plot Data, *Remote Sensing of the Environment* **32**: 91-101, 1990.

Bruegge, C. J. J. E. Conel et al., In-situ atmospheric water-vapor retrieval in support of AVIRIS calibration, *SPIE - Imaging Spectroscopy of the Environment* **1298**: 150-163, 1990.

Carder, K. L. W. W. Gregg et al., Determination of Saharan Dust radiance and chlorophyll from CZCS imagery, *Journal of Geophysical Research* **96**(D3): 5369-5378, 1991.

Chester, R. (1990). Marine Geochemistry. London, Unwin Hyman.

D'Almeida, G. A. P. Koepke and E. P. ShettleA. Deepak (1991). Atmospheric Aerosols: Global Climatology and Radiative Characteristics. Hampton, VA, A. Deepak Publishing.

Darzi, M. and J. W. Winchester, Aerosol characteristics at Mauna Loa Observatory, Hawai'i, after east Asian dust storm episodes, *Journal of Geophysical Research* **87**(C2): 1251-1258, 1982.

Duce, R. A. (1986). The impact of atmosphere nitrogen, phosphorous, and iron species on marine biological productivity. The Role of Air-Sea Exchange in Geochemical Cycling. P. Buat-Menard. Hingham, Mass., D. Reidel**:** 497-529.

Ehsani, A. R. (1992)., Ph.D. dissertation, Design of a microprocessor based sun-tracking multi-channel solar radiometer system. Department of Electrical Engineering. Tucson, University of Arizona**:** 129.

Elterman, L. (1968). UV, Visible, and IR Attenuation for Altitudes to 50 km, Department, Office of Aerospace Research, USAF. Bedford, Massachusetts, AFCRL-68-0153.

Gordon, H. R. (1996). MODIS Normalized Water-leaving Radiance Algorithm Theoretical Basis Document, Department, University of Miami. Coral Gables, FL, MOD 18.

Gordon, H. R. O. B. Brown et al., A semianalytic radiance model of ocean color, *Journal of Geophysical Research* **93**(C9): 10,909-10,924, 1988.

Gordon, H. R. and D. J. Castaño, Coastal Zone Color Scanner atmospheric correction algorithm: multiple scattering effects, *Applied Optics* **26**(11): 2111-2122, 1987.

Gordon, H. R. and D. K. Clark, Clear water radiances for atmospheric correction of coastal zone color scanner imagery, *Applied Optics* **20**(24): 4175-4179, 1981.

Gordon, H. R. D. K. Clark et al., Phytoplankton pigment concentrations in the Middle Atlantic Bight: comparison of ship determinations and CZCS estimates, *Applied Optics* **22**(1): 20-36, 1983.

Gordon, H. R. and M. Wang, Surface-roughness considerations for atmospheric correction of ocean color sensors. I: The Rayleigh-scattering component, *Applied Optics* **31**(21): 4247-4260, 1992.

Gordon, H. R. and M. Wang, Influence of oceanic whitecaps on atmospheric correction of ocean-color sensors, *Applied Optics* **33**(33): 7754-7763, 1994.

Gordon, H. R. and M. Wang, Retrieval of water-leaving radiance and aerosol optical thickness over the oceans with SeaWiFS, *Applied Optics* **33**: 443-452, 1994.

Gregg, W. W. and K. L. Carder, A simple spectral solar irradiance model for cloudless maritime atmospheres, *Limnology and Oceanography* **35**(8): 1657-1675, 1990.

Holben, B. N. T. F. Eck et al., Automatic sun and sky scanning radiometry system for network aerosol monitoring, *Remote Sensing of the Environment* **in press**, 1996.

Hurst, V. J., Visual estimation of iron in saprolite, *Geological Society of America Bulletin* **88**: 174-176, 1977.

Junge, C. (1963). Air Chemistry and Radioactivity, Academic Press.

Kasten, F. and T. Young, Revised optical air mass tables and approximation formula, *Applied Optics* **28**(22): 4735-4738, 1989.

Kaufman, Y. J. A. Gitelson et al., Size distribution and scattering phase function of aerosol particles retrieved from sky brightness measurements, *Journal of Geophysical Research* **99**(D5): 10,341-10,356, 1994.

Lindberg, J. D. and L. S. Laude, Measurement of the absorption coefficient of atmospheric dust, *Applied Optics* **13**(8): 1923-1926, 1974.

Martin, J. H. K. H. Coale et al., Testing the iron hypothesis in ecosystems of the equatorial Pacific Ocean, *Nature* **371**(6493): 123-129, 1994.

Martin, J. H. and S. E. Fitzwater, Iron deficiency limits phytoplankton growth in the north-east Pacific subarctic, *Nature* **331**: 341-343, 1988.

Merrill, J. T. R. Bleck and L. Avila, Modeling atmospheric transport to the Marshall Islands, *Journal of Geophysical Research* **90**(D7): 12,927-12,936, 1985.

Nakajima, T. G. Tonna et al., Use of sky brightness measurements from ground for remote sensing of particulate polydisperions, , 1996.

Patterson, E. M., Optical properties of the crustal aerosol: relation to chemical and physical characteristics, *Journal of Geophysical Research* **86**(C4): 3236-3246, 1981.

Patterson, E. M. and D. A. Gillette, Commonalities in measured size distribution for aerosols having a soil-derived component, *Journal of Geophysical Research* **82**(15): 2074-2082, 1977.

Patterson, E. M. C. S. Kiang et al., Global Measurements of Aerosols in Remote Continental and Marine Regions: Concentrations, Size Distributions, and Optical Properties, *Journal of Geophysical Research* **85**(C12): 7361-7376, 1980.

Powell, K. A. C. R. Trepte and G. S. Kent (1996). Observations of Saharan dust by LITE. Advances in Atmospheric Remote Sensing with Lidar, 18th ILRC, Berlin.

Prospero, J. M. (1981). Arid Regions as sources of mineral aerosols in the marine atmosphere. Desert Dust: Origin, Characteristics, and Effect on Man. T.L. Péwé. Boulder, CO, Geological Society of America. **1:** 303.

Rahn, K. A. (1976). The chemical composition of the atmospheric aerosol, Department, University of Rhode Island. Kingston, Rhode Island, Technical Report.

Reinersman, P. N. and K. L. Carder, Monte Carlo simulation of the atmospheric point spread function with application to correction for adjacency effect, *Applied Optics* **34**(21): 4453-4471, 1995.

Savoie, D. L. (1978)., Ph.D. dissertation, Physical and chemical characteristics of Saharan aerosols over the tropical Northern Atlantic. Coral Gables, University of Miami**:** 137.

Savoie, D. L. and J. M. Prospero, Saharan aerosol transport across the Atlantic Ocean: characteristics of the input and the output, *Bull. Am. Met. Soc.* **57**: 145, 1976.

Schmid, B. and C. Wehrli, Comparison of Sun photometer calibration by use of the Langley technique and the standard lamp, *Applied Optics* **34**(21): 4500-4512, 1995.

Schütz, L. R. Jaenicke and H. Pietrek (1981). Saharan dust transport over the North Atlantic Ocean. Desert Dust: Origin, Characteristics, and Effects on Man. T.L. Péwé. Boulder, CO, Geological Society of America.

Shettle, E. P. and R. W. Fenn (1979). Models for the Aerosols of the Lower Atmosphere and the Effects of Humidity Variations on Their Optical Properties, Department, Air Force Geophysics Laboratory, AFGL-TR-79-0214.

Van de Hulst, H. C. (1957). Light Scattering by Small Particles. New York, John Wiley & Sons, Inc.

Wang, M. and H. R. Gordon, Retrieval of the columnar aerosol phase function and single-scattering albedo from sky radiance over the ocean: simulations, *Applied Optics* **32**(24): 4598-4609, 1993.

Wang, M. and H. R. Gordon, Estimation of aerosol columnar size distribution and optical thickness from the angular distribution or radiance exiting the atmosphere: simulations, *Applied Optics* **34**(30): 6989-7001, 1995.

Wendisch, M. and W. von Hoyningen-Huene, High speed version of the method of "Successive Order of Scattering" and its application to remote sensing, *Beitr. Phys. Atmosph.* **64**(2): 83-91, 1991.

Winker, D. M. R. H. Couch and M. P. McCormick, An overview of LITE: NASA's Lidar In-space Technology Experiment, *Proc. IEEE* **84**(2): 164-180, 1996.

Young, R. W. K. L. Carder et al., Atmospheric Iron Inputs and Primary Productivity: Phytoplankton Responses In The North Pacific, *Global Biogeochemical Cycles* **5**(2), 1991.

APPENDICES

Appendix A: Clear Water Radiances at Chlorophyll Concentrations < 2.0 mg/m^3

In the oligotrophic ocean (found typically between 35 °N and 35 °S), where chlorophyll *a* concentrations are less than 0.25 mg m^{-1}, the remote-sensing reflectance, R_{rs}, and normalized water-leaving radiance, L_{wn}, can be predicted with an 8% error for wavelengths longer than 500 nm (Gordon and Clark, 1981). Preliminary data (see diagram) suggest that $R_{rs}(510)$ and $R_{rs}(531)$ can be predicted with about a 13% error for waters with chlorophyll concentrations of up to 2.8 mg $m^{-.3}$.

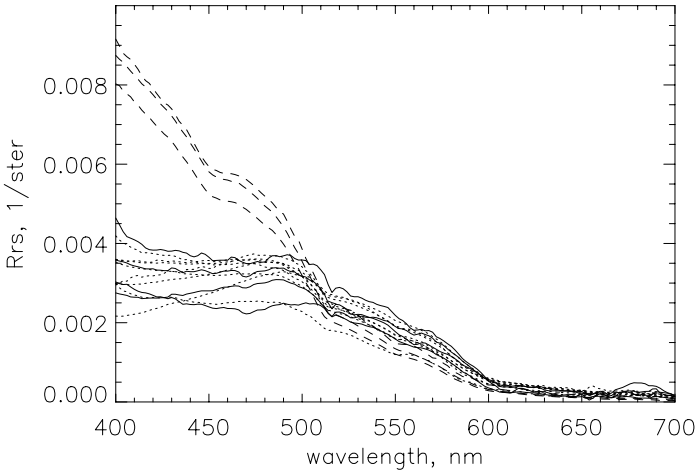

$R_{rs}(\lambda)$ vs. λ for 12 stations in the Gulf of Mexico and near Iceland with chlorophyll concentrations ranging from 0.07 to 2.8 mg m^{-3} (mean 0.58) have a mean ± standard deviation at 510 and 531 nm of 0.00264 ± 0.00032 and 0.00216 ± 0.00029, respectively. This yields an estimate of a 12% to 13% error in R_{rs} (and thus in L_{wn}) at 510 or 531 nm (the error is about 17% for 551 nm).

R_{rs} can be converted into L_{wn} via $L_{wn}(\lambda) = R_{rs}(\lambda)\, F_0(\lambda)$, where F_0 is the incoming extraterrestrial solar irradiance. The mean value of $L_{wn}(551)$ for the data in Fig. 3 is 0.313 mW cm^{-2} μm^{-1} sr^{-1}, which is nearly the same as the $L_{wn}(550)$ value of 0.30 mW cm^{-2} μm^{-1} sr^{-1} that was used for clear-water atmospheric correction in the processing of CZCS data (Gordon et al., 1983).

We hope to extend the use of "clear-water" radiances to regions with chlorophyll concentrations as high as 0.5-1.0 mg/m^3. For major dust outbreaks where the major flux of iron to the ocean might be expected, $L_{as}(531)$ will be far greater than the increase in uncertainty in $L_w(531)$.

***Appendix B*: Diagram of atmospheric scattering components**

10-15% of Rayleigh scattering molecules, and 70-80% of the aerosol particles are normally found . below 2 km (*Elterman 1968; Wang and Gordon 1993*). For computational purposes, then, the atmosphere may be divided into two layers, as illustrated in the following diagram:

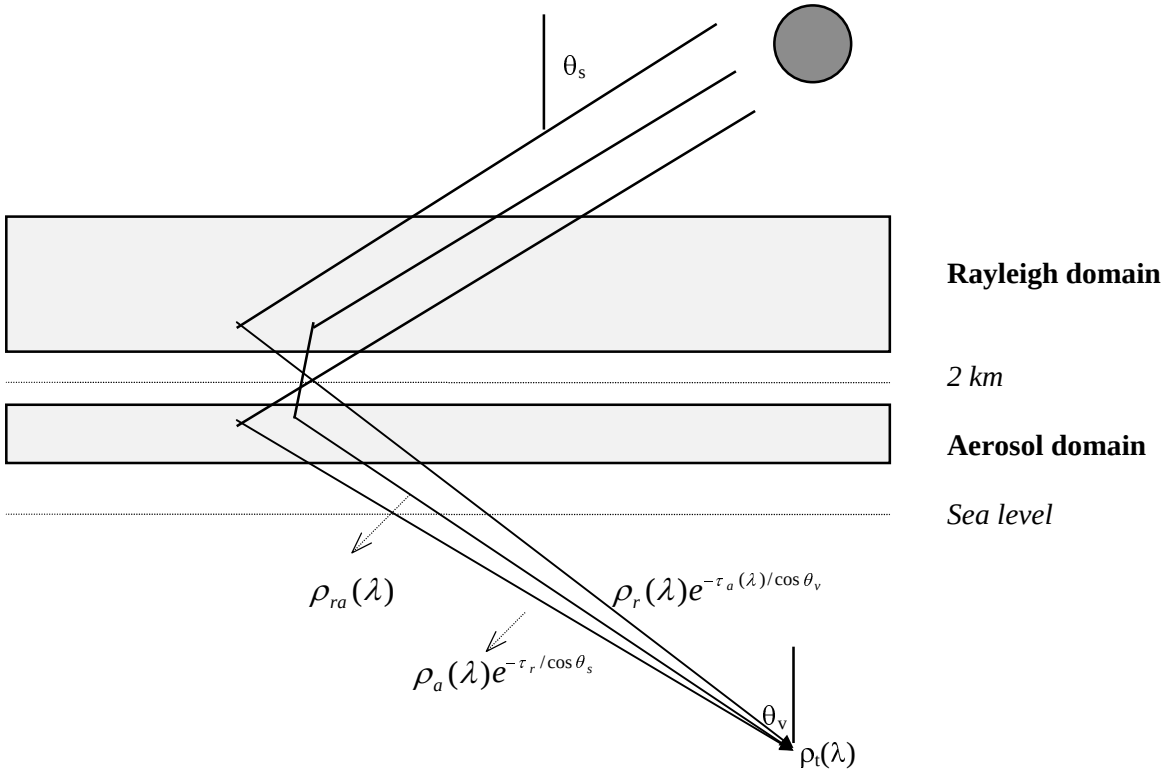

ρ_{ra} = radiance from interaction between aerosols and air molecules
ρ_r = radiance from scattering by air molecules without presence of aerosol layer
ρ_a = radiance from scattering by aerosols without presence of air molecules
ρ_t = total radiance received at the sensor
$\tau_{r,a}$ = Rayleigh and aerosol optical thicknesses, respectively
$\theta_{v,s}$ = Viewing and solar zenith angles, respectively

Hence, the total signal may be expressed as

$$\rho_t(\lambda) = \rho_r(\lambda)e^{-\tau_a(\lambda)/\cos\theta_v} + \rho_a(\lambda)e^{-\tau_r(\lambda)/\cos\theta_s} + \rho_{ra}(\lambda)$$

APPENDIX C: Validation of Saharan Dust model

The effects of phase functions of aspherical particles, atypical atmospheric vertical profiles, and the determination of absorption and scattering light histories are more accurately obtained through Monte Carlo computations than by packaged radiative transfer programs containing inherent assumptions. Measured optical depths, meteorological variables, and estimates of the vertical dust profile (*Schütz et al. 1981*) will be used with field radiance data to retrieve the scattering phase function and albedo of Saharan dust. Consistent agreement of model results with multiple dust events should indicate a successful optical characterization of a long-range Saharan aerosol. The asphericity of the particles may also be investigated by comparing the retrieved scattering phase function with the size distribution obtained from aerosol samples (see Aerosol Samples).

Field Methods (Ft. Jefferson, Dry Tortugas)

Given the solar angle, a nadir-viewing sensor may be simulated by observing the backscattered signal at a chosen spectroradiometer viewing angle. Typically, a nadir-viewing sensor will observe backscattering angles from approximately 80-130°; the radiometer data was taken to simulate such angles. The following diagram illustrates the geometry:

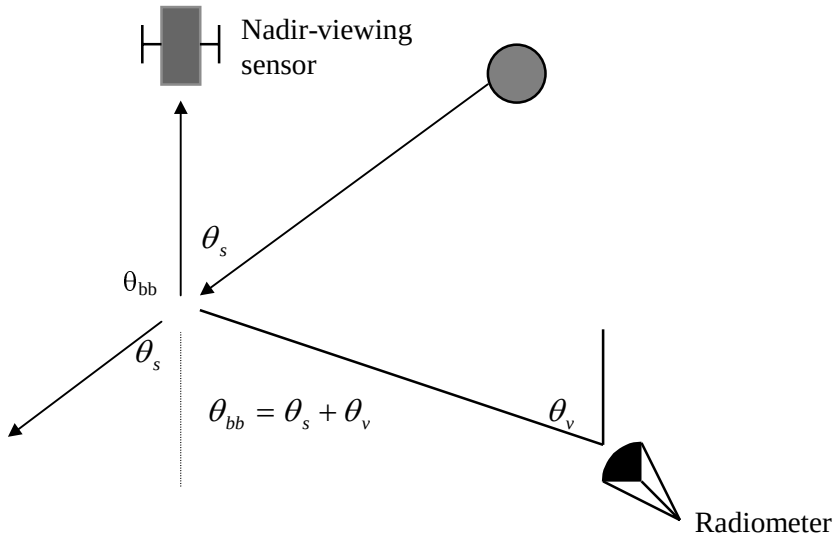

Principal plane data have been collected to date at Ft. Jefferson, Dry Tortugas during dust events in June and July 1996, July 1997, and on clear days in March 1996 and January 1997. Ft. Jefferson is an island site 70 miles west of Key West, sufficiently free of anthropogenic influence but southerly enough

to experience frequent passage of Saharan dust in the summer months. The dust events are tracked by GOES and Meteosat images available on the internet to monitor trajectories and anticipated arrival times.

Instrumentation & Calibration

Sun photometer

The Reagan radiometer is an automated, temperature stabilized, sun photometer that follows the solar disk over all zenith and azimuthal angles at 10 channels in the visible spectrum chosen to avoid significant gaseous absorption lines in the atmosphere (380.5, 399, 441, 520, 609, 669, 781, 869, 939, 1028.5 nm). The 609 and 939 channels provide estimates of ozone and columnar water vapour, respectively. Each channel has a FWHM transmission bandpass varying between 8 and 12 nm, and 0.05° tracking uncertainty (*Ehsani 1992*).

The calibration constant of a sun photometer, $V_o(\lambda)$, is determined by the Langley plot (*Biggar et al. 1990; Bruegge et al. 1990; Schmid and Wehrli 1995*), in a dry, cloud-free, stable atmosphere at a high altitude to eliminate most of the aerosols contained in the MBL. The attenuated solar irradiance, E_s, reaching the Earth's surface over an Earth-Sun distance, R (given in AU), is given by,

$$E_s = \frac{E_{so}}{R^2} e^{-\tau m},$$

where *m* is the airmass. The solar irradiance received at the detector is directly proportional to the voltage produced. A Langley-Bouger plot,

$$\ln(V) = \ln(\frac{V_o}{R^2}) - \tau m,$$

yields a slope equal to the total optical depth and the zero airmass voltage V_o from the y-intercept. The US Naval Observatory's Almanac for Computers is used to correct for atmospheric refraction, and Kasten's equation (*Kasten and Young 1989*) to determine airmass in the optical depth retrieval.

Spectrometer

The Ocean Optics Lab of the University of South Florida has designed and constructed a compact, versatile spectrometer known unofficially as the Spectrix (designation SPX). The Spectrix

utilizes a holographic grating to split the incident signal onto a 512 channel, large area, linear array detector. A mechanical shutter is utilized for true dark current. The spectral range is 350-900 nm and the field-of-view is 2.5° when a 50 mm field stop is used. In order to accurately assess the viewing angle, a digital protractor (accuracy 0.1°) is attached to a camera head alongside the Spectrix.

Preliminary calibration of the Spectrix is performed in a laboratory darkroom using a NIST-traceable tungsten lamp. The Licor, mentioned below, is placed at the distance quoted in the lamp specifications, and again at 15 inches away in order to determine the diminution of lamp intensity over that distance. A calibrated panel is then placed perpendicular to the source at this distance. The Spectrix is placed close, and 45°, to the panel; 7-10 scans are taken and averaged to give the calibration curve.

A calibration sphere with a 3-4% NIST-traceable accuracy will be purchased shortly to provide a more uniform radiance source for calibration.

Solar-based calibration data were taken by viewing a calibrated Spectralon panel at Mt. Lemmon on an extremely clear day, and are currently being processed. These data will provide better accuracy in the blue-UV portion of the spectrum than do tungsten lamps with a blackbody temperature near 3100 K. Concurrent optical depth and meteorological measurements will be used as inputs to a radiative transfer code to compute the downward irradiance for each measurement set. Given the bi-direction reflectance (BRF) of the calibrated panel, the ratio to form the calibration coefficients may then be obtained.

Irradiance Meter

The Licor LI-1800 is a self-contained spectroradiometer that scans 300-850 nm at 4 nm resolution. Calibration is achieved using the NIST-traceable tungsten lamp at a prescribed distance. Calibration data from Mt. Lemmon are also being processed; a solar-based calibration should improve calibration in the blue wavelengths.

A Spectrix scan of the Spectralon grey card is being investigated as a viable surrogate for irradiance. The BRDF and scan angles of the card are critical to the calibration accuracy and are under investigation.

Primary Data

Optical Depths

Instantaneous total optical depths may be derived using the above Langley-Bouger technique and the derived calibration intercept,

$$\tau_{inst} = \frac{\ln\left(\frac{V_0}{R^2}\right) - \ln(V)}{m},$$

An iterative method (*Biggar et al. 1990*) is used to determine the Junge parameter and estimated ozone amount for a stable atmosphere in the morning or afternoon; this method is considered a more accurate estimation of the Junge parameter since 9 wavelengths are used to model the aerosol. This method will not be as valid during periods of high turbidity due to dust since the optical depths are often not log-linear (see Field Methods) and the atmosphere unstable. Therefore, care must be taken to maintain frequent and accurate calibrations of the radiometers to reliably determine the instantaneous aerosol optical depths.

Sky Radiance

Skylight scattering measurements are taken in the solar principal plane rather than solar almucantar measurements that are more commonly used in aerosol *in situ* scattering measurements and modeling (*Gordon and Wang 1994; Kaufman et al. 1994*). The Spectrix allows us to scan no closer than 6° from the sun's centre. In the principal plane, 3 scans are taken at each 5° interval from approximately 160° to 6°. The largest scattering angles are taken first to accomodate the rapid changes in the solar zenith angle. We consider angular increments of 5° as an optimal tradeoff between a comprehensive scattering data set with a 2.5° FOV, yet allows each data set to be collected in a period of time over which the atmosphere may be considered stable. Each set of measurements takes approximately 20 minutes. Very clear conditions and Monte Carlo code may allow for the range of valid angles to exceed 160°. The azimuthal orientation of the radiometer is adjusted every few measurement sets to ensure it still lies in the principal plane. Scans of a characterized grey panel are also taken periodically to determine downwelling irradiance to determine reflectances that may be used in the data reduction, avoiding error resulting from the radiometric calibration.

Downwelling Irradiance

The BRDF and low sun angle present during collection times may prevent the use of a characterized Spectralon card as a measure of irradiance. The validity of these grey-card scans are under investigation from measurements taken in January and March 1997. It seems likely that any error introduced by scanning the card for reflectance measurements will be less than that of the absolute calibration of the Spectrix and the Licor.

Ancillary Data

A Campbell Scientific meteorological package, with a CR500 datalogger, records the barometric pressure (±2 mb, 0-40°C, 600-1060 mb), temperature (±0.2°C, -35°C to +50°C), and relative humidity (±3%) at sampling intervals identical to the Reagan radiometer (usually 1 minute).

Monte Carlo modeling

Multiple scattering considerations

Multiple scattering is significant in sky radiance measurements at all visible wavelengths and scattering angles (*Nakajima et al. 1996*). The radiance from multiple scattering , however, varies continuously and is well- behaved over all scattering angles (*Wendisch and von Hoyningen-Huene 1991*). This behaviour allows multiple scattering in ground-based measurements to be estimated as a function of aerosol optical depth and viewing geometry (*Wang and Gordon 1993*). In this latter study, the Rayleigh-aerosol interaction term at longer wavelengths was found to be almost insensitive to the aerosol model (see panel *a* below): sensitivity to the aerosol model increased with decreasing wavelength. These results suggest that multiple scattering effects at specified solar and azimuthal angles (principal plane measurements) may be successfully determined at the longer wavelengths where little absorption by dust will be present. Once the scattering phase function has been estimated, investigations by Monte Carlo calculations of the phase

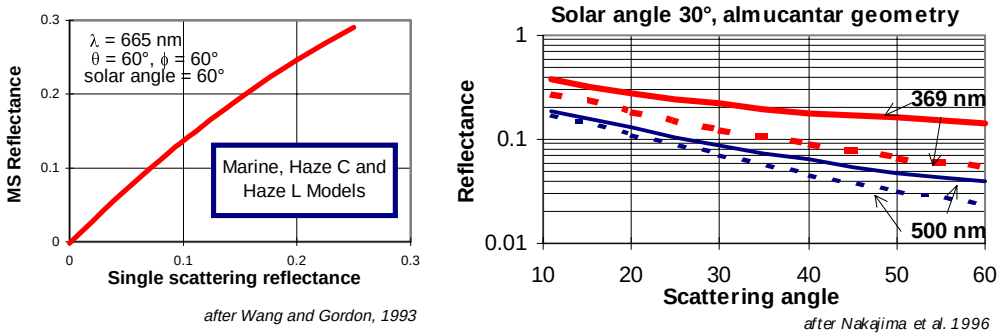

Panel a. Multiple & single scattering reflectance vs. pure single-scattering reflectance for wavelength and viewing geometry shown. The results are almost identical for all three aerosol models. Wang and Gordon's paper indicated that multiple scattering may be accurately estimated and removed from radiometric data given viewing geometry and wavelength in the red wavelengths; knowledge of the aerosol model becomes more critical in the blue wavelengths. ***Panel b.*** Aerosol reflectance retrievals from almucantar data using single-scattering assumptions (solid line) and after accounting for multiple scattering (dotted line) with $\tau_a(500)=0.5$, ground albedo A=0.20, a refractive index of 1.5-0.01i, and a radius interval of 0.05 - 20 microns. The retrieved reflectances continue converging at angles less than 10°. The marked difference already present at these lower scattering angles indicates multiple scattering will dominate the received signal at much greater scattering angles.

function and albedo will be extended into the dust absorption regime (380-500 nm; see next sections)

Retrieval Scheme

The proposed scheme to retrieve the scattering phase function is to first estimate the multiple scattering at the given solar and viewing angles and measured optical depths for the longer sun photometer wavelengths (670, 780, 870, 1030 nm. This will be done using a LUT approach similar to Gordon's except that measurements in the principal plane rather than the solar almucantar will be simulated when generating this reference table. The red wavelengths will be used first because little or no absorption is expected in these bands, and the multiple scattering is largely independent of the aerosol model for this regime. The Rayleigh radiance, and multiply scattered radiance are then removed, leaving the singly scattered aerosol radiance. This is then fit using a two-term Henyey-Greenstein phase function with an albedo close to unity. The unmeasured part of the scattering spectrum (approximately 160° - 180°) would need to be extrapolated from the 130 - 160° data. A Monte Carlo simulation is then performed using the initial guess of the scattering phase function. The difference between experimental and simulated sky reflectance would dictate the change required in scattering phase function or albedo, prompting a new Monte Carlo simulation with the improved phase function. Once Monte Carlo simulations agree with the field reflectance, a full Monte Carlo simulation and/or other radiative transfer code will be run to achieve a final result. 5-10 iterations are expected. *Wang and Gordon (1993)* found 10 iterations to be sufficient to reduce disagreement between simulated radiometric data and the derived optical parameters to 1%.

Preliminary data reduction

Initial data taken during June and July of 1996 has been reduced using a single scattering approximation in order to determine the feasibility of using principal plane data using the Spectrix sensitivity and FOV. A two-layer atmospheric model (*Gordon and Wang 1994*) was used to separate the Rayleigh and aerosol scattering regimes,

$$\rho_t(\lambda) = \rho_r(\lambda)e^{-\tau_a(\lambda)/\cos\theta_v} + \rho_a(\lambda)e^{-\tau_r(\lambda)/\cos\theta_s} + \rho_{ra}(\lambda), \text{ where}$$

$$\rho_x(\lambda) = \frac{\pi L_x(\lambda)}{F_o(\lambda)\cdot\cos\theta_o}, \text{ and } L_x(\lambda) = \frac{F_o(\lambda)\omega_o(\lambda)\tau_x(\lambda)P_x(\Theta,\lambda)}{4\pi\cdot\cos\theta_v}$$

Sample plots of the retrieved albedo-phase function products shown below are therefore given by,

$$\omega_o(\lambda)P_a(\Theta,\lambda) = \frac{4\pi\cos\theta_v}{F_o(\lambda)\tau_a(\lambda)}\left[\rho_t(\lambda) - \rho_r(\lambda)e^{-\tau_a(\lambda)/\mu}\right]e^{\tau_r(\lambda)/\mu_o},$$

assuming no multiple interaction ($\rho_{ra} = 0$). Optical depths are obtained from the Reagan radiometer. The smoothly varying curves and dynamic range of the data illustrate the capability of the instrumentation to perform principal plane measurements. The contribution from multiple interactions is very significant at 520 nm where we observe a greatly elevated signal at large scattering angles.

Gordon and Wang's simulated data have shown retrieval accuracy near 5% using principal plane measurements (120-150°) and 2-3% with use of almucantar data at smaller scattering angles, suggesting that our error in the principal plane will be only slightly increased over the almucantar approach.

The optical depths for days in June and July 1996 during suspected dust events are shown on the following page. Also included is a clear day observed at Islamorada, Florida Keys in March of the same year, where a marine aerosol dominated the clear atmosphere. The sky radiance data were taken at the

same times on June 1 and 3 during a passage of a dust event. June 3 is used as the clear day comparison even though optical depths are still elevated and optically controlled by the dust. When dust concentrations

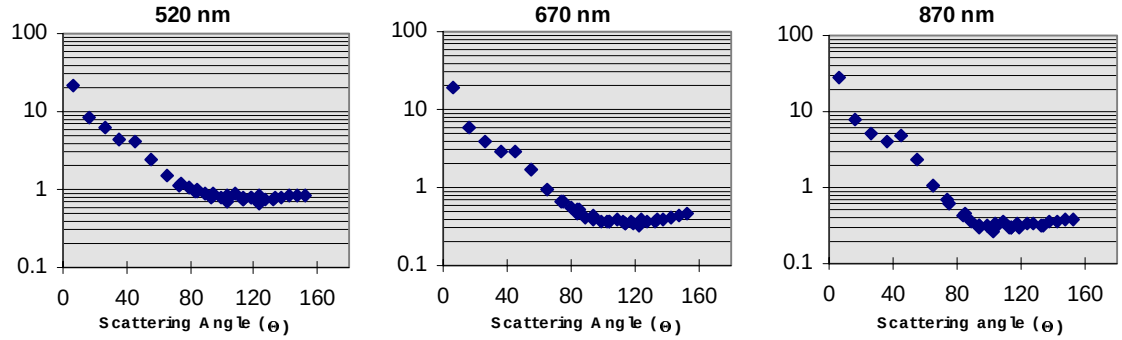

Panels a-c. Plots of w(λ)P(Θ,λ) vs. scattering angle (Θ) at three wavelengths for dust event on June 3, 1996 at Ft. Jefferson, Dry Tortugas.

were much higher on June 1, an increase in sky radiance was seen at the green and red wavelengths, as expected, but a *decrease* was observed in the blue wavelengths. This reduction also increased with scattering angle (and thus with multiple scattering). The radiance is normalized by the downwelling irradiance in order to account for the extraterrestrial solar irradiance, gaseous absorption, and to eliminate instrumental calibration uncertainties,

$$L_{norm}(\lambda) = \frac{L_{radiometer}(\lambda)}{E_d(0^+,\lambda)} = \frac{\pi L_{radiometer}(\lambda)}{\pi F_o(\lambda)\cdot\cos\theta_o \cdot t(\lambda)} \equiv \frac{1}{\pi \cdot t(\lambda)}\rho_t(\lambda)$$

Thus, the normalized radiance is similar to reflectance, but also includes the diffuse transmittance t(λ).

The near-forward scattering peak of large dust particles is very strong; hence the Rayleigh-aerosol multiple s*cattering* term will produce only small changes in the total radiance from a clear to dusty day, and would not affect the received signal in such a dramatic manner. Absorption of light by dust will increase with multiple interactions since a greater number of opportunities for absorption with the same albedo leads to greater total absorption of light; we infer the observed reduction of blue light to be due to absorption by the aerosol through single and multiple interactions.

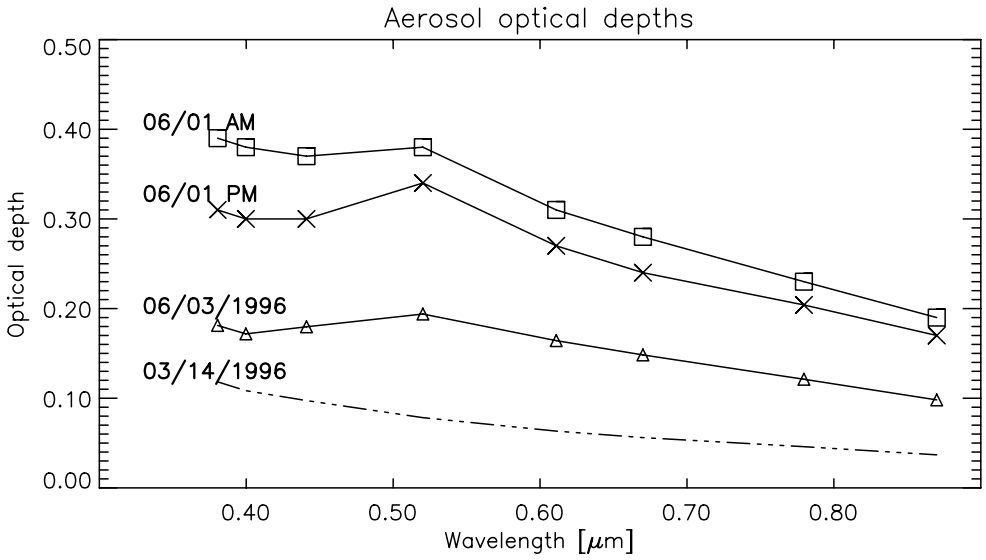

Aerosol optical depths for the dust event observed during June 1996 (solid lines) at Ft. Jefferson, Dry Tortugas. Included for reference is a clear day dominated by a marine aerosol observed at Islamorada, Florida Keys (dotted line) in March 1996. The rapid decrease in optical depths over the 3-day period in June is interpreted as the passage of a trailing edge of the dust storm. The sharp peaks in optical depth at the 520 wavebands are believed to be due to a unimodal size distribution overwhelming the signal from any other aerosols present.

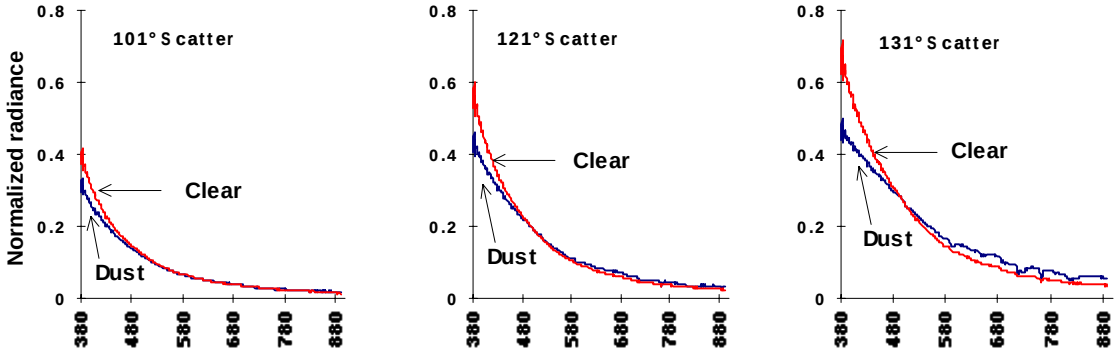

Panels a-c. Sky radiance vs. wavelength on June 1 (dust) and June 3 (clear), 1996. The sky radiance is normalized by a grey panel scan to eliminate most atmospheric absorption effects. The denotation *normalized* distinguishes it from *reflectance*. Each scattering angle experienced a reduction in blue light (380-500 nm) during the dust event, but increased signal at the higher wavelengths due to increased scattering.

The radiometric data show that principal plane measurements at large scattering angles promise to be a sensitive indicator of the presence of spectrally absorbing aerosols.

Aerosol samples

Drs. Savoie and Prospero of the University of Miami's AEROCE project have agreed to send aerosol samples collected daily at Barbados and Miami on request (*Arimoto et al. 1995*). They have, in fact, already delivered aerosol samples collected from May 30-June 6 and July 10-16, 1996, the two Saharan dust events encountered last year. Marine aerosols are well characterized, and will only be requested once on a comparative basis, but samples requested for periods covering each dust event, with two days on either side of the event should be representative of the dust aerosol present over Ft. Jefferson during the field data collection (D. Savoie, pers. comm.) The reflectance and imaginary part of the index of refraction will be determined on these samples using the method , Patterson et al. (1980).

Size distribution analysis

The aerosol samples are collected on Whatman-41 cellulose ashless filters. The samples will be ashed to remove the filters and prepared for a scanning electron microscope (SEM) analysis (*Betzer et al. 1988*). Computer software allows for a quick and comprehensive size distribution analysis. The samples are expected to be markedly aspherical; I will likely choose to classify particles by an area-equivalent diameter. The sphere-equivalent size distribution will be run through the Mie scattering program to determine and compare the derived to the field-retrieved scattering phase functions.

Chemical analysis

Part of the received sample will be prepared for energy-dispersive analysis by X-ray (EDAX). The relative elemental abundance of the sample can be determined. Classification schemes will be set up to estimate the chemical structure/type of particle using relative abundances. Types of clay present should be estimable from previous work. Combining The EDAX and SEM results will yield an idea of the relative abundances of each aerosol type (marine, dust, anthropogenic, clay). A new system has been purchased by USF and processing is beginning.

These samples will give an idea of the morphology and chemistry of the particles in question. It is not meant as, and will not be, a comprehensive study. These SEM investigations will, however, allow visual evidence of the nonsphericity of the particles, give an idea of the magnitude of its effect upon scattering, and possibly allow a correlation of the derived albedo to the relative concentration of iron present on the coating of the dust particle.

Products

These investigations are expected to produce several primary results:

1. An optical characterization of a Saharan dust aerosol that has undergone long and medium range transport.
2. An improved determination of chlorophyll pigment concentration in images where such dust is present
3. Detailed histories of absorption and scattering in the presence of dust, as functions of scan and view angles, aerosol optical depths, aerosol model.
4. A possible estimation of iron flux to the ocean.

The derived optical characteristics and characteristic epsilon will afford their use in MODIS and SeaWiFS image correction, with guesses based upon climatology and region. Saharan dust closer to source regions and Gobi dust can be characterized once this method has proven successful for long-range Saharan dust. The unimodal size distribution expected for long-range Saharan dust will simplify this particular investigation.